HIGHLIGHTS FROM CMS*

Hwi Dong Yoo

on behalf of the CMS Collaboration

Seoul National University, Seoul, South Korea
hdyoo@cern.ch

(Received May 19, 2017)

We report on highlights for recent physics results from the CMS experiment. All results are based on proton–proton collision data at $\sqrt{s} = 8$ or 13 TeV collected by the CMS detector. This report contains various interesting topics and their latest results at the CMS: Standard Model (SM) physics including Quantum Chromodynamics (QCD), Electroweak (EWK), and top and bottom quarks, Higgs physics, and beyond SM (BSM) searches such as Supersymmetry (SUSY) and non-SUSY exotic searches.

DOI:10.5506/APhysPolB.48.1237

1. Introduction

The CMS Collaboration consists of about five thousands members globally from 200 institutions and 43 countries. During Run 1 (2010–2012), the CMS detector has successfully operated and, finally, a Higgs boson has been discovered [1, 2]. After a long shutdown from 2013 to 2014, Run 2 started at $\sqrt{s} = 13$ TeV and the CMS has collected around 40 fb^{-1} data in 2015 and 2016, more than initial expectations. More than 570 papers have been published and submitted using Run 1 and Run 2 datasets. In this paper, we report on the latest CMS results for various topics based on $\sqrt{s} = 8$ and 13 TeV datasets.

2. SM physics

2.1. QCD

These measurements are important to constrain models and higher order calculations such as next-to-next-to-leading order (NNLO) and hadronization models in order to improve the knowledge of parton distribution functions (PDFs). For example, measurements of the inclusive jet cross section,

---

* Presented at the Cracow Epiphany Conference "Particle Theory Meets the First Data from LHC Run 2", Kraków, Poland, January 9–12, 2017.

jet multiplicities, jet correlations, to understand the difference between forward and central productions, strong coupling constant ($\alpha_{\rm s}$), jet production mechanism in association with EWK bosons and heavy flavour jets (bottom or charm quark) have been studied recently at the CMS. In such measurements, pileup severely impacts many channels utilising calorimeter-based objects. Therefore, a lot of efforts are on-going to improve the understanding of the pileup effect at the CMS.

The inclusive jet cross sections are measured using datasets with various centre-of-mass energy such as $\sqrt{s}$ = 2.76, 8 and 13 TeV. The results are presented as a function of jet transverse momentum ($p_{\rm T}$) with different rapidity (y) and compared to predictions of perturbative QCD at next-to-leading order (NLO) using various sets of PDFs. Figure 1 shows the results for the three different datasets. The inclusive jet production cross section, measured at $\sqrt{s}$ = 2.76 TeV (top left), 8 TeV (top right), and 13 TeV (bottom left and right) are shown as a function of jet $p_{\rm T}$ in various rapidity bins as indicated by different symbols. The statistical (systematic) experimen-

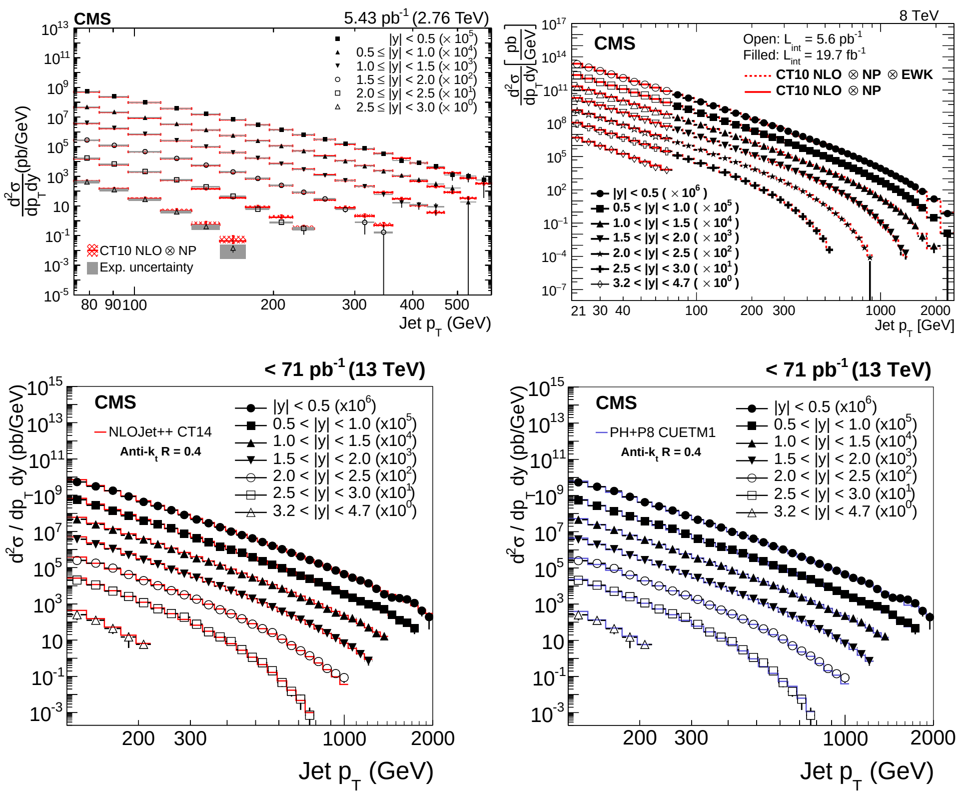

Fig. 1. Various results of the inclusive jet production cross section [3–5].

tal uncertainties are indicated by vertical error bars (filled bands). These measurements are compared to the following NLO QCD predictions: CT10 PDF set (top left), CT10 PDF set corrected for the non-perturbative (NP) factor for the low p_{T} data and the NP and EWK correction factors for the high p_{T} data (top right), NLOJet++ based on CT14 PDF set corrected for the NP and EWK effects (bottom left), and POWHEG+PYTHIA 8 with tune CUETM1 (bottom right).

The strong coupling constant is extracted from different measurements at high-momentum scale like up to TeV. Deviation at this scale could appear due to BSM. Figure 2 shows the running of the α_{s} as a function of the scale Q, obtained by using the CT10 NLO PDF set. The solid line and the uncertainty band are obtained by evolving the extracted $\alpha_{\mathrm{s}}(M_Z)$ values. The dashed line indicates the evolution of the world average value.

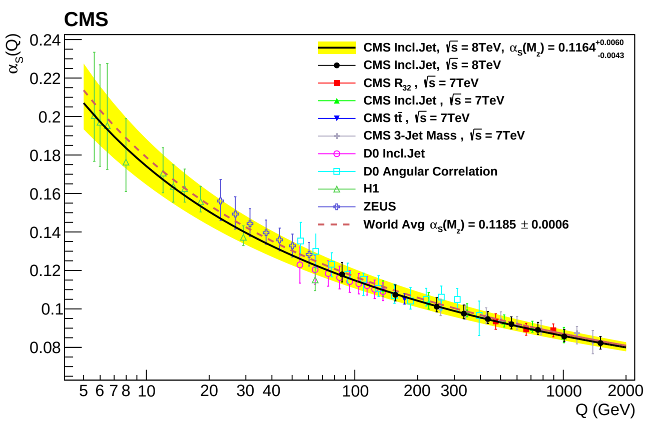

Fig. 2. Results of α_{s} from various CMS measurements [4].

2.2. EWK

CMS has delivered increasingly precise measurements of single, di-, and multi-boson production cross sections. Single boson production measurements provide tests of higher order QCD calculations and constraints of PDFs. In particular, EWK induced asymmetries in W decays have been precisely measured over a large rapidity intervals allowing for strong constraints on the PDFs from the LHC. In addition, the Drell–Yan (DY) process is an important SM benchmark channel allowing for tests of the NNLO perturbative QCD calculations and it is a major background for various BSM searches in leptonic channels. Figure 3 shows the results of W charge asymmetry (left) and Drell–Yan differential cross section (right). Comparison of the asymmetries and differential cross sections to NNLO predictions calculated using the FEWZ 3.1 interfaced with different PDF sets are also shown.

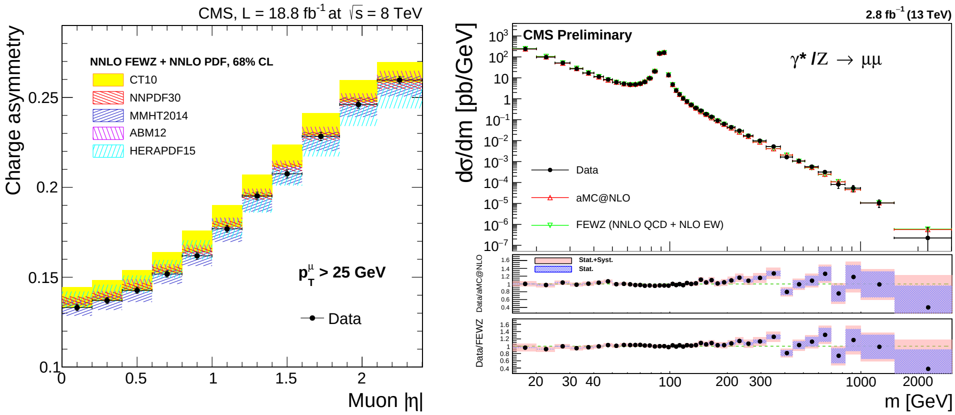

Fig. 3. Results of W charge asymmetries at $\sqrt{s} = 8$ TeV (left) [6] and Drell–Yan differential cross section at $\sqrt{s} = 13$ TeV (right) [7].

Studies of di-boson and multi-boson productions like WW, WZ, ZZ, di-photon and tri-boson productions are motivated to test EWK theory and can be important backgrounds to various Higgs and BSM searches. Also the studies provide indirect sensitivities to BSM-like anomalous triple and quartic gauge couplings (aTGC and aQGC). The following measurements allow access to rare processes and provide sensitive probes: di-boson production (aTGC), tri-boson production (aQGC), single boson production via vector boson fusion (aTGC), and vector boson scattering (aQGC). Figure 4 shows the summary of many di-boson measurements obtained with the recent CMS datasets. Results are consistent with theoretical predictions indicated with grey/yellow bands in the plot.

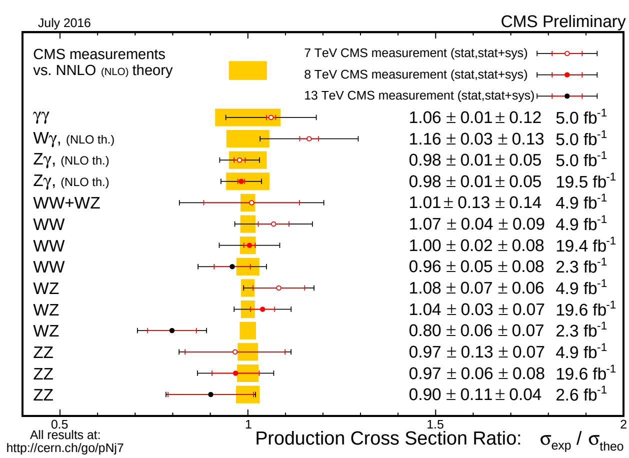

Fig. 4. (Colour on-line) Summary of EWK multi-boson production cross sections [8].

2.3. Top-quark physics

The top quark has been discovered in 1995 at the Tevatron, however, the properties of the top quark still need further understanding. It is crucial to improve the precision of inclusive and differential top-quark production cross-section measurements and it needs to be done in multiple dimensions. With this improvement, we can constrain PDFs and test new improved higher order QCD calculations and sophisticated new MC generators on the top-quark production. Moreover, exploring the coupling of the top quark to W, Z and H will provide huge sensitivities for BSM, which are analysed in the framework of the effective field theory (EFT). In addition, we look for rare production processes, such as four or six top-quark productions.

Precise measurements on the $t\bar{t}$ production cross sections in leptonic and hadronic channels are performed. The purpose of these precision measurements is to find deviations which could be due to BSM contributions. So far, no significant excess beyond the SM predictions is observed. Also precise understanding of the top-quark mass is connected to the Higgs originality and BSM. The result of the top-quark mass measurements based on $\sqrt{s} = 7$ and 8 TeV datasets outperforms the precision of the world best combination performed in 2014. Figure 5 shows the various results of $t\bar{t}$ production cross sections (left) and top-quark mass (right) measurements.

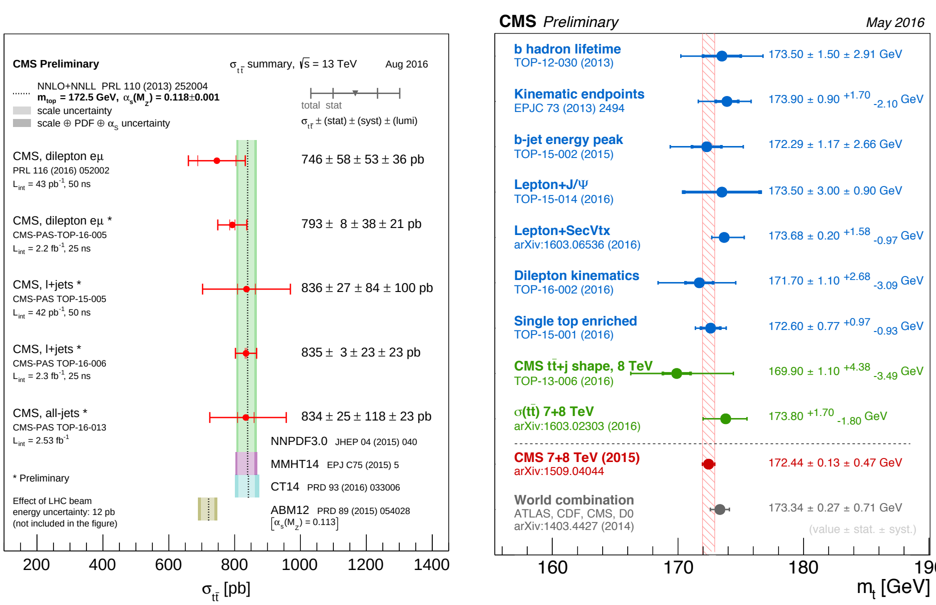

Fig. 5. Summary of $t\bar{t}$ production cross sections (left) and top-quark mass (right) measurements [9].

Measurement of the differential and double-differential cross sections for $t\bar{t}$ production at 13 TeV has been performed using the dataset corresponding to an integrated luminosity of 2.3 fb^{-1}. The $t\bar{t}$ cross section is measured in the lepton+jets channel with $t\bar{t}$ p_{T}, rapidity, invariant mass, and the number of additional jets in the system. The measurement at the parton level is dominated by the uncertainties in the parton shower and hadronization modelling, therefore, the comparisons with various theoretical models are also performed. The dependence on these theoretical models is reduced for the particle-level measurement. In general, the results are slightly lower than predictions, but within the uncertainty compatible with the expectation. The results are shown in Fig. 6.

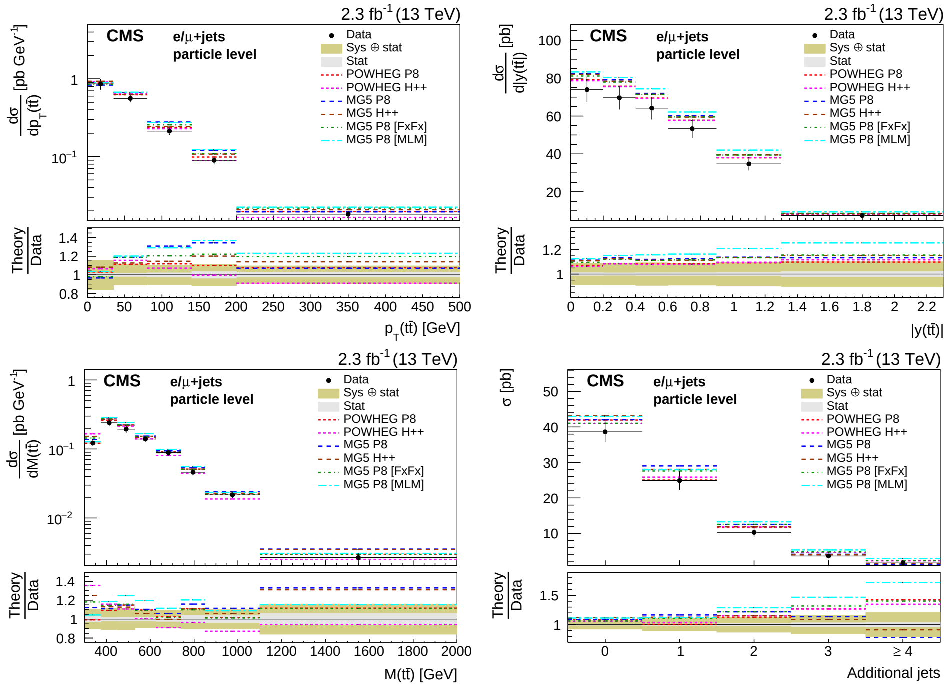

Fig. 6. Differential cross sections at particle level as a function of $t\bar{t}$ p_{T} (top left), rapidity (top right), invariant mass (bottom left), and cross sections as a function of the number of additional jets (bottom right) [10].

3. Higgs physics

Higgs analyses are a main physics program of the CMS experiment. Obviously, the Higgs physics is very sensitive to new physics which can be achieved by precision measurements or by looking in areas of increased sensitivity.

With Run 2 data, the Higgs boson has been rediscovered by the ZZ (decaying to four leptons) and $\gamma\gamma$ final states. Local significances are 6.2σ in the ZZ channel and 6.0σ in the $\gamma\gamma$ channel respectively. These studies are performed using a dataset corresponding to an integrated luminosity of 12.9 fb^{-1} at $\sqrt{s} = 13$ TeV. A search for additional resonances in the channels are studied for a range of masses up to TeV scale and with various widths. No significant excess beyond the SM prediction is observed. Figure 7 shows the distributions of the four lepton (left) and di-photon (right) reconstructed invariant mass after event selection.

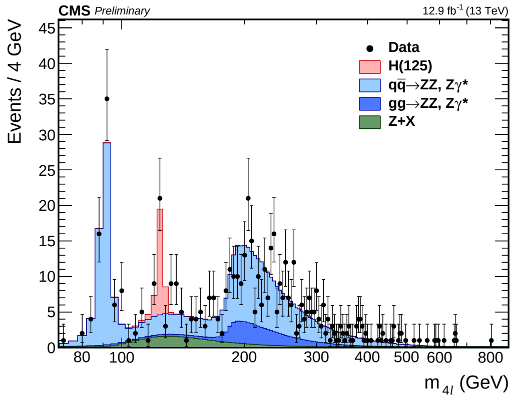

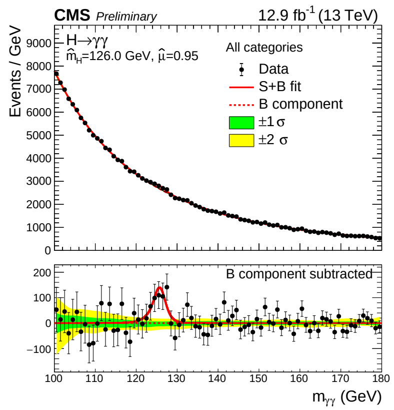

Fig. 7. Distributions of the four-lepton (left) [11] and di-photon (right) [12] reconstructed invariant mass in the Higgs mass range.

We also present a search for the associated production of an SM Higgs boson and a $t\bar{t}$ pair ($t\bar{t}H$). The dataset corresponds to an integrated luminosity of 12.9 fb^{-1}. In this study, two leptons of the same charge or at least three charged leptons are used, and at least one of the leptons should come from the top quarks. b jets appear in the final state and the Higgs boson decays into WW^*, ZZ^* and $\tau\tau$ are only considered. The results are shown in Fig. 8. Left plot shows the comparison between data and SM prediction for the selected leptons which are in a good agreement. 95% C.L. upper limit on the signal production cross section is set and the signal strength is 2.0 times the SM prediction. The right plot in Fig. 8 shows best fit signal strength for the combined 2015+2016 analysis and flavour categorised results.

In addition, the search for the production of a pair of Higgs bosons in various final states such as $bbbb, bb\gamma\gamma, bbWW$, and $bb\tau\tau$ has been performed. Searches in the channel containing two photons and two bottom quarks, both resonant and non-resonant production of the Higgs bosons are performed, using the dataset corresponding to 2.7 fb^{-1} at $\sqrt{s} = 13$ TeV. In Fig. 9, expected and observed upper limits are shown. The observed data is in an agreement with SM predictions.

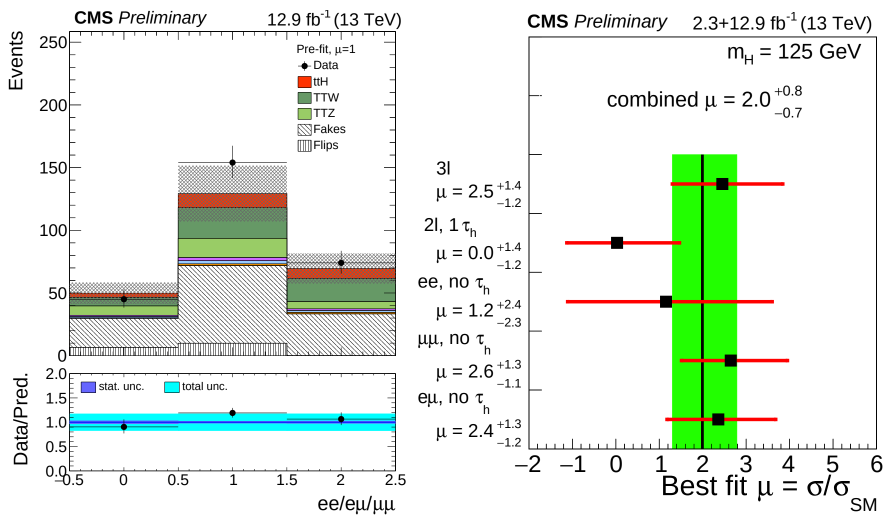

Fig. 8. Comparison between data and prediction for the selected leptons in the same-sign di-lepton channels: from left to right $ee, e\mu, \mu\mu$ (left). Best fit signal strength for the combined 2015 and 2016 analysis in the di-lepton and tri-lepton channels with flavour categories (right) [13].

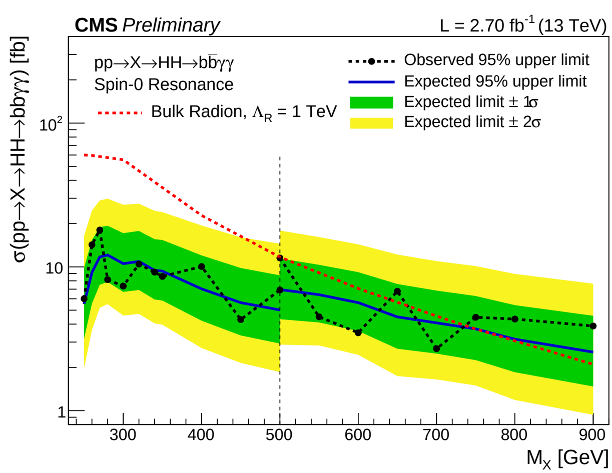

Fig. 9. Expected and observed upper limits on the production of $pp \to HH \to b\bar{b}\gamma\gamma$ for the resonant analysis [14].

4. Exotic searches

4.1. SUSY searches

SUSY provides a more fundamental symmetry from the theoretical point of view, a solution to the hierarchy problem and it can be a candidate of dark matter (DM). In the SUSY, SM particles have a SUSY partner from which it differs in spin by one-half. Production mechanism of the SUSY is characterised by the strong production of squarks and gluinos, direct production of third generation squarks and EWK production. Strong production of coloured superpartners provides largest cross sections and, therefore, can be observed first. The generic signature based on this production contains missing transverse energy (MET), jets and leptons in the final state. The results for the searches are shown in Fig. 10. The left plot shows limits on the gluino pairs decaying to four top quarks categorised by the number of leptons in the final state. The right plot shows the limits in the light quark final states.

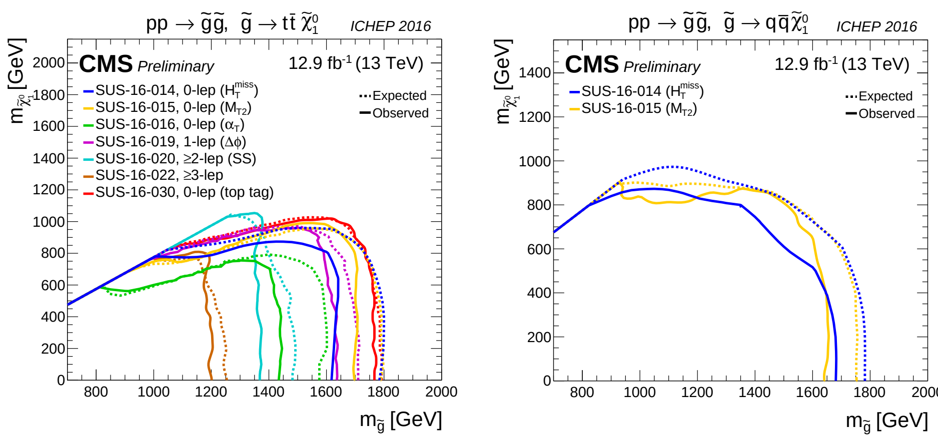

Fig. 10. Limits on gluino pairs decaying into four top quarks (left) and light quarks (right) by strong production [15–22].

Third generation squark, such as stop and sbottom is also studied. More advanced techniques are employed in this search and the event signature from signal models are similar to SM $t\bar{t}$ background. The results on the limit for this search is shown in Fig. 11 (left). EWK SUSY productions are accessible at higher luminosity because of small couplings. This search typically does not have a jet associated and it provides a different event signature compared to other searches. Therefore, searches for the production can be complementary to searches described earlier, although the cross section is lower than for strong production. Many channels are explored and limit results are shown in Fig. 11 (right).

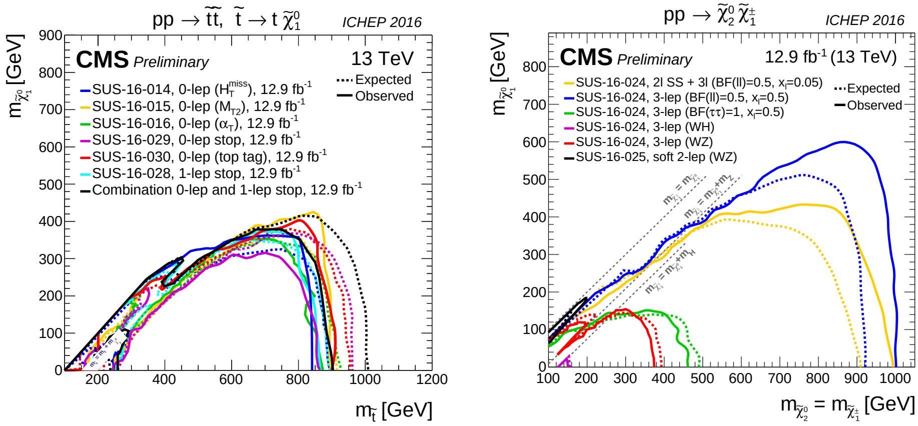

Fig. 11. Limits on stop pairs decaying into 2 top quarks (left) and EWK-ino production (right) [15–18, 22–24].

4.2. Non-SUSY searches

Searches for a high-mass resonance in di-lepton channel is a key analysis for various BSM searches based on the leptonic final state. Many theoretical models predict such a high-mass resonance, for example, the sequential SM (SSM) and the grand unification theories (GUT) inspired models. This di-lepton channel provides a very clean event signature at the TeV scale. Dominant SM backgrounds are DY processes decaying into two leptons. This search is performed in the di-electron and di-muon mass spectra using the dataset corresponding to the integrated luminosity of 12.4 fb^{-1} and 13.0 fb^{-1}. No significant excess is observed from the SM prediction. Figure 12 shows the di-electron and di-muon invariant mass spectra respectively. Upper limits are set on the di-lepton invariant mass distribution shown in Fig. 13. We obtain lower mass limits of 4.0 TeV (SSM) and 3.5 TeV (GUT) respectively.

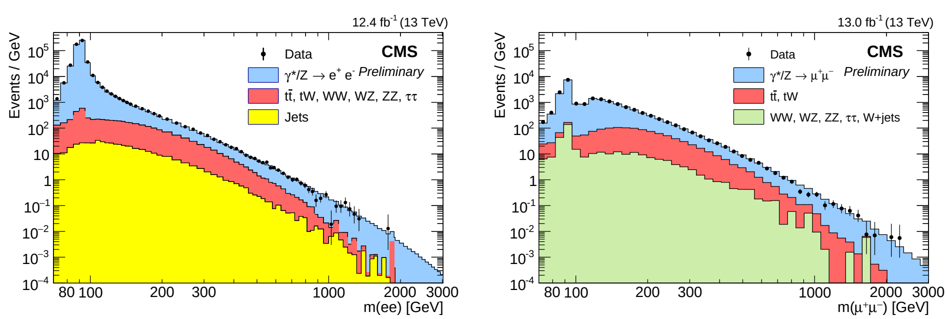

Fig. 12. The invariant mass spectra of di-electron (left) and di-muon (right) events after applying event selection [25].

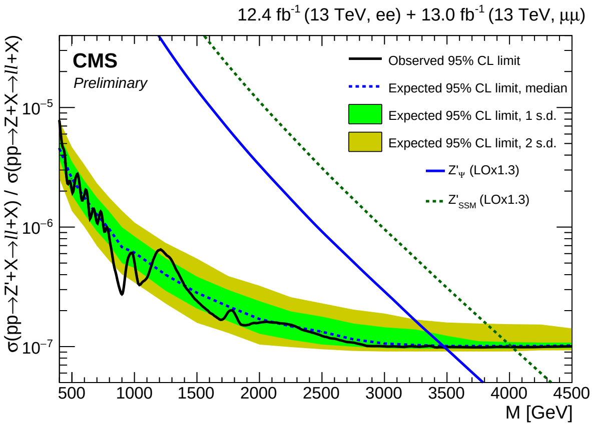

Fig. 13. The 95% C.L. upper limits on the production cross section times branching fraction for a spin-1 resonance, relative for a Z boson, for the combined di-electron and di-muon channels [25].

A similar search is studied in the di-jet final state using the same dataset. A low-mass search is based on calorimeter jets and a high-mass search is based on particle-flow jets. The di-jet invariant mass spectra are smoothly falling distribution, therefore, they are described by a smooth parametrisation. Figure 14 shows the results: di-jet mass spectrum (left) and upper

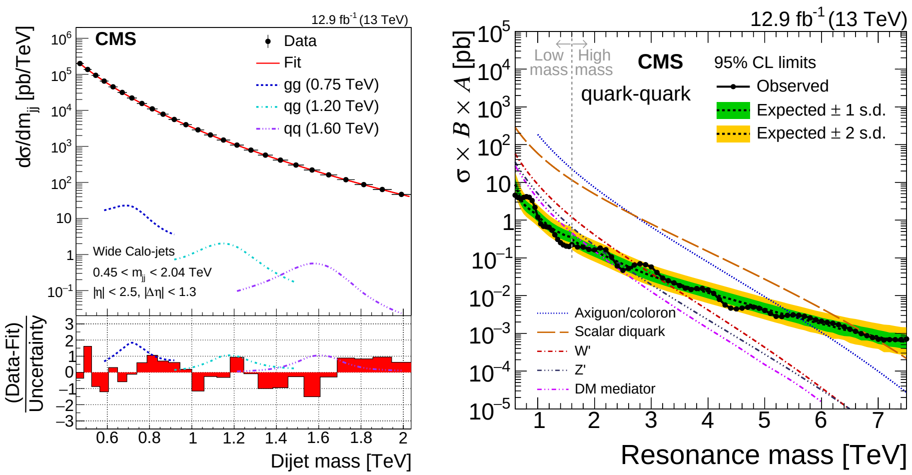

Fig. 14. Di-jet mass spectrum compared to a fitted parametrisation of the background for the low-mass search (left). The observed 95% C.L. upper limits on the production cross section, branching fraction, and acceptance for quark–quark type di-jet resonances (right) [26].

limits on the production cross section (right) up to 7.4 TeV with various theoretical models such as a scalar quark, string, colorons, excited quarks, *etc.* No evidence for such resonances are observed.

A search for the resonant production of high-mass photon pairs are performed with a dataset collected at 2015. Both ATLAS and CMS have observed non-negligible excesses at around 750 GeV in di-photon channel with 3.9σ (ATLAS) and 3.4σ (CMS) local significances in a spin-0 scenario [27, 28]. These results have provided a huge impact in the community on both the theoretical and experimental sides, and many interesting discussions have been followed to explain such excesses. The same search is performed with larger dataset corresponding to 12.9 fb^{-1} collected by the CMS detector in 2016. The same analysis strategy is applied and two energetic photons in the final state are selected. The results are shown in Fig. 15. The left plot shows the observed di-photon invariant mass spectrum and the right plot shows the p-value with background-only hypotheses. No significant deviation is observed beyond the SM prediction.

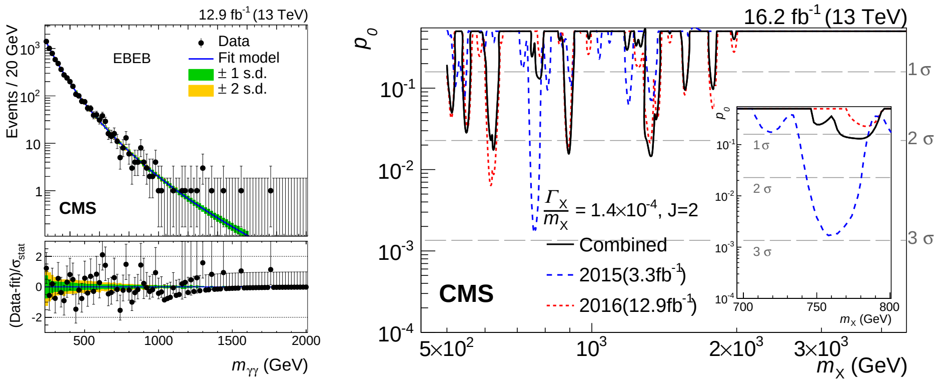

Fig. 15. The observed invariant mass spectrum of di-photon for selected events in the EBEB category (left). Observed background-only p-value for narrow resonances as a function of the resonance mass, from the combined analysis of data recorded in 2015 and 2016 (right) [29].

A similar search for a heavy resonance is performed in the $Z\gamma$ final state, where one photon is replaced by a Z boson. In this search, only a Z boson decaying to a di-electron or di-muon is considered. This search has the same strategy as the di-photon search discussed earlier, which fits the di-lepton and a photon invariant mass distribution with the background modelling above 300 GeV through an unbinned likelihood method. This analysis is performed using the dataset corresponding to the integrated luminosity of 12.9 fb^{-1} at $\sqrt{s} = 13$ TeV. Figure 16 shows the fit results of the invariant mass spectrum in the di-electron (left) and di-muon (right) channels, respectively, and Fig. 17 shows the combined limit on the production cross section. No significant excess beyond the SM prediction is observed.

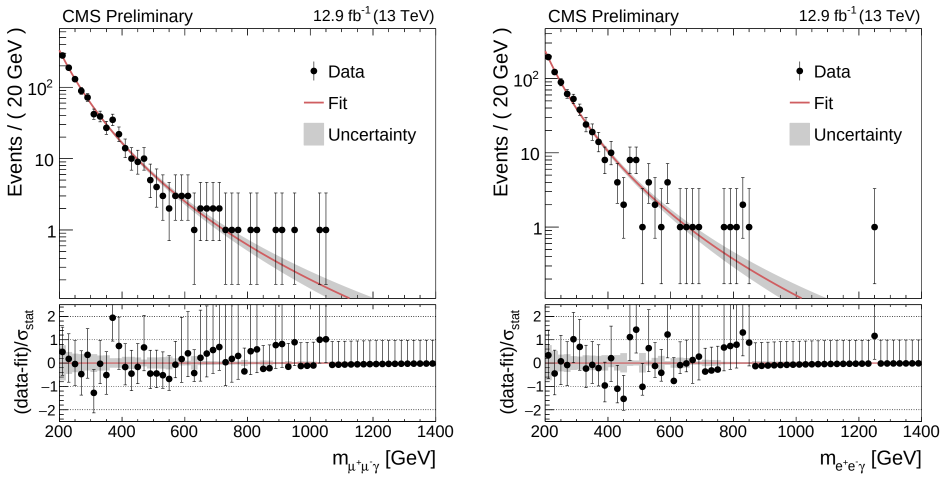

Fig. 16. Fits of the $m_{Z\gamma}$ distribution in the data for the di-electron (left) and di-muon (right) channels [30].

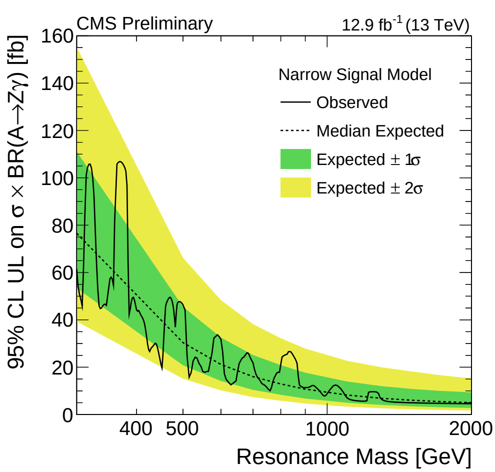

Fig. 17. Observed and expected 95% C.L. exclusion limits on $\sigma(A \to Z\gamma)$ as a function of signal mass in the background-only hypothesis and combination of di-electron and di-muon channels [30].

4.3. DM searches

DM is one of the main mysteries in current particle physics. A large amount of indirect evidence shows the existence of DM but it had not been directly observed yet. Therefore, many searches have been performed in last few decades. The DM can be also searched at the LHC. Typically DM particles are invisible in the detector. However, total transverse momentum should be conserved in an event. Using this feature, events with visible particles from the initial state radiation with large MET can be a candidate of event signature from the DM particles. These are referred to as "mono-X" searches, where "X" can be a jet, photon, Z/W boson, Higgs boson, *etc.*

In Run 1, mono-X searches have been mostly done in terms of EFT via contact interaction, which is valid if the mediator mass is much larger than momentum transfer. However, this scenario is not valid at a high-energy transfer, therefore in Run 2, we considered another set of scenarios using simplified models. In this scenario, higher momentum transfer is possible and we can define mediator particles explicitly.

Searches for DM particles with a jet (mono-jet) or a photon (mono-photon) with large MET are performed. In these searches, there is at least one energetic jet or photon in the final state without any lepton contribution. The mono-jet search provides the largest cross section but it suffers by huge SM backgrounds from DY process with the initial-state gluon radiation. The

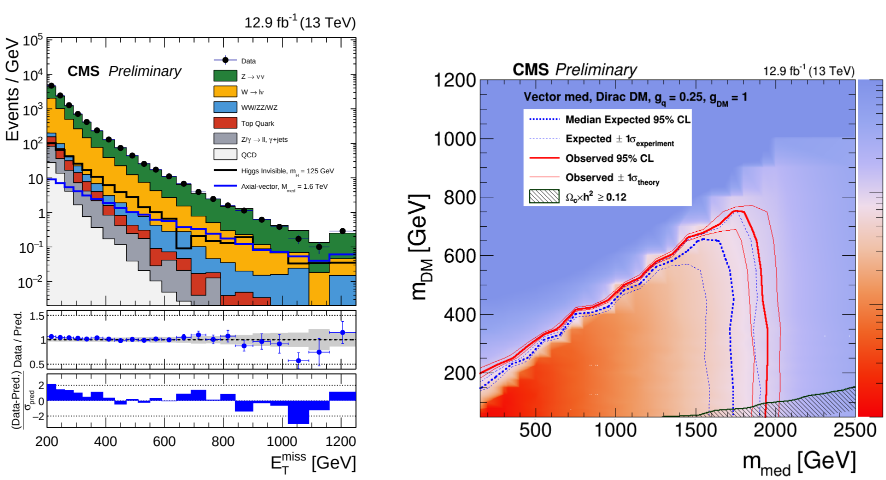

Fig. 18. Observed MET distribution in the mono-jet signal regions compared with the post-fit background estimations for various SM processes (left). Exclusion limits at 95% C.L. on the $\mu = \sigma/\sigma_{\text{theory}}$ in the m_{med}–m_{DM} plane for a vector mediator (right). Expected and observed exclusion contours are overlaid, where mass points to the lower left of the curves are excluded [31].

mono-photon search has relatively smaller cross section than the mono-jet search but it provides cleaner event signature in the final state than mono-jet due to the photon requirement. The analysis is studied using the dataset corresponding to the integrated luminosity of 12.9 fb^{-1}. Figures 18 and 19 show the results of the mono-jet and mono-photon searches. The left plot in each figure shows the observed MET distribution after event selection. The distribution from data is in a good agreement with the SM predictions. The right plot in each figure shows the upper limits in the mono-jet and photon searches and provides the strong constraints on the dark matter pair production cross section through vector and axial–vector mediators. No significant excess is observed in both channels.

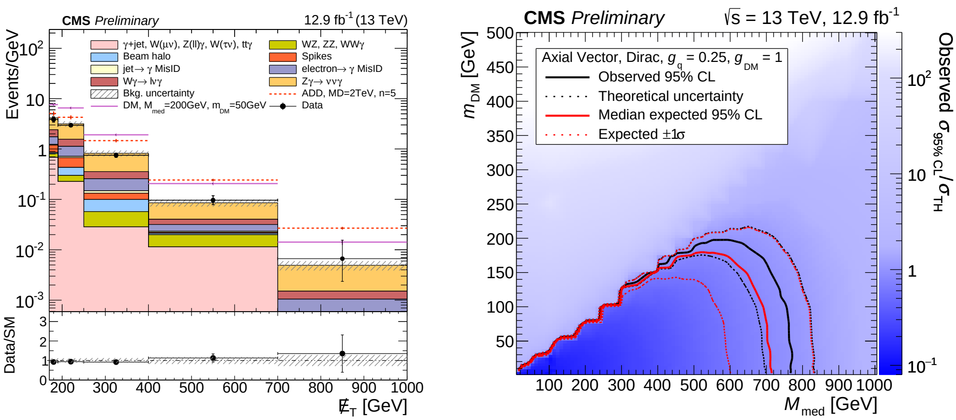

Fig. 19. Observed MET distribution in the mono-photon signal regions compared with background estimations for various SM processes (left). 95% C.L. upper limits on $\mu = \sigma/\sigma_{\text{theory}}$ in the m_{med}–m_{DM} plane for a vector mediator, assuming $g_q = 0.25$ and g_χ (right). Expected and observed exclusion contours are overlaid, where mass points to the lower left of the curves are excluded [32].

5. Summary

We discussed a large number of recent results for both SM precision measurements including Higgs physics and BSM searches using dataset collected by the CMS detector. The datasets considered were taken in 2012, 2015 and 2016. The CMS Collaboration is very active in various physics topics. So far, there has been no significant evidence beyond SM predictions in any channel. However, many interesting analyses are being studied and all possible scenarios are being probed with latest dataset taken in 2016 corresponding to the integrated luminosity of around 36 fb^{-1}. New results will be presented in upcoming conferences during this year and exciting observations may be presented in the new results.

H.D. Yoo is supported in part by the National Research Foundation of Korea (NRF) funded by the Korea government (NRF-2015R1C1A1A0105 3087 and NRF-2015R1A4A1042542).

REFERENCES

[1] CMS Collaboration, *Phys. Lett. B* **716**, 30 (2012).

[2] ATLAS Collaboration, *Phys. Lett. B* **716**, 1 (2012).

[3] CMS Collaboration, *Eur. Phys. J. C* **76**, 265 (2016).

[4] CMS Collaboration, *J. High Energy Phys.* **1703**, 156 (2017).

[5] CMS Collaboration, *Eur. Phys. J. C* **76**, 451 (2016).

[6] CMS Collaboration, *Eur. Phys. J. C* **76**, 469 (2016).

[7] CMS Collaboration, CMS-PAS-SMP-16-009, `cds.cern.ch/record/2205152`

[8] CMS Collaboration, `https://twiki.cern.ch/twiki/bin/view/CMSPublic/PhysicsResultsCombined`

[9] CMS Collaboration, `https://twiki.cern.ch/twiki/bin/view/CMSPublic/PhysicsResultsTOPSummaryFigures`

[10] CMS Collaboration, *Phys. Rev. D* **95**, 092001 (2017) [`arXiv:1610.04191 [hep-ex]`].

[11] CMS Collaboration, CMS-PAS-HIG-16-033, `cds.cern.ch/record/2204926`

[12] CMS Collaboration, CMS-PAS-HIG-16-020, `cds.cern.ch/record/2205275`

[13] CMS Collaboration, CMS-PAS-HIG-16-022, `cds.cern.ch/record/2205282`

[14] CMS Collaboration, CMS-PAS-HIG-16-032, `cds.cern.ch/record/2207960`

[15] CMS Collaboration, `https://twiki.cern.ch/twiki/bin/view/CMSPublic/PhysicsResultsSUS`

[16] CMS Collaboration, CMS-PAS-SUS-16-014, `cds.cern.ch/record/2205158`

[17] CMS Collaboration, CMS-PAS-SUS-16-015, `cds.cern.ch/record/2205162`

[18] CMS Collaboration, CMS-PAS-SUS-16-016, `cds.cern.ch/record/2205163`

[19] CMS Collaboration, CMS-PAS-SUS-16-019, `cds.cern.ch/record/2204932`

[20] CMS Collaboration, CMS-PAS-SUS-16-020, `cds.cern.ch/record/2204929`

[21] CMS Collaboration, CMS-PAS-SUS-16-022, `cds.cern.ch/record/2205165`

[22] CMS Collaboration, CMS-PAS-SUS-16-030, `cds.cern.ch/record/2204930`

[23] CMS Collaboration, CMS-PAS-SUS-16-028, `cds.cern.ch/record/2205271`

[24] CMS Collaboration, CMS-PAS-SUS-16-029, `cds.cern.ch/record/2205276`

[25] CMS Collaboration, CMS-PAS-EXO-16-031, `cds.cern.ch/record/2205764`

[26] CMS Collaboration, *Phys. Lett. B* **769**, 520 (2017) [`arXiv:1611.03568 [hep-ex]`].

[27] CMS Collaboration, *Phys. Rev. Lett.* **117**, 051802 (2016).

[28] ATLAS Collaboration, *J. High Energy Phys.* **1609**, 1 (2016).

[29] CMS Collaboration, *Phys. Lett. B* **767**, 147 (2017).

[30] CMS Collaboration, CMS-PAS-EXO-16-034, `cds.cern.ch/record/2204921`

[31] CMS Collaboration, `arXiv:1703.01651 [hep-ex]`.

[32] CMS Collaboration, CMS-PAS-EXO-16-039, `cds.cern.ch/record/2205148`